THE JOURNAL OF PHYSICAL CHEMISTRY C

Article

pubs.acs.org/JPCC

Sub-Kelvin Collision Temperatures in Merged Neutral Beams by Correlation in Phase-Space

Yuval Shagam and Edvardas Narevicius*

Department of Chemical Physics, Weizmann Institute of Science, Rehovot 76100, Israel

ABSTRACT: Recent merged neutral beam experiments have introduced the possibility of measuring reactive collisions in the cold regime down to 10 mK. The lowest temperature attained in these experiments cannot be explained using the standard formalism developed for crossed molecular beam scattering. These low temperatures become accessible because pulsed supersonic beams develop a correlation in velocity-position space during free propagation such that the local velocity standard deviation decreases. This effect is responsible for a reduction in the attainable collision energy by more than 2 orders of magnitude along with an order of magnitude improvement in the resolution. We show that supersonic nozzles with short pulsed opening durations compared to the time-of-flight, such as the Even-Lavie valve, have a clear advantage in achieving low collision energies with improved resolution. We discuss possible improvements in the energy resolution by varying the detection time duration.

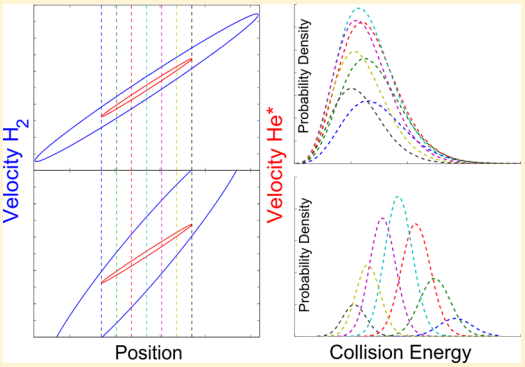

1. INTRODUCTION

The Chemical Physics community has been striving to realize reactions in the cold regime below 1 K for many years. Quantum effects become dominant at these temperatures where the typical interaction length scale approaches the de Broglie wavelength of the reactants. Resonances in reaction rates are formed when particles tunnel through centrifugal or reaction barriers,[1] and Wigner threshold laws set the behavior of reaction cross sections at these low energies.[2]

The pioneering work of Herschbach and Y. T. Lee set the stage for gas phase reactive scattering studies using crossed molecular beam configurations with collision temperatures exceeding 100 K.[3−5] Orbiting resonances were observed in this temperature range by cleverly choosing collision partners for which these resonances appear at relatively high energies.[6,7] Later, by varying the angle between the beams Toennies and collaborators were able to reach collision temperatures above 5 K.[8] Since then, many different avenues have been explored, attempting to reach even colder temperatures. These include CRESU (Cinétique de Réaction en Ecoulement Supersonique Uniforme) experiments where the reactants are seeded in a supersonic expansion ensuring thermal equilibrium.[9−11] Another school of thought uses buffer gas cooling to realize these cold collisions.[12,13] Additional methods have been used to study inelastic collisions, by incorporating Stark deceleration[14] into crossed-beam configurations.[15−18] Alternative promising methods, which can be used to control colliding beam velocities, include Zeeman,[19,20] optical,[21] mechanical,[22] and moving trap deceleration.[23,24] Further cooling techniques could subsequently be applied, such as single-photon cooling,[25,26] to reach well into the cold regime.

Only a small number of experiments have reported reactive collision temperatures at or below 1 K,[13,27−30] either with laser cooled or buffer gas cooled reactants. Recently we have realized this goal by measuring cold Penning ionization reactions down to 10 mK utilizing a merged supersonic beam setup.[31] Employing merged supersonic beams for cold reactions was also theoretically proposed and analyzed by Wei et al.[32] In the model presented in Wei et al.,[32] the collision energy and resolution are defined by the velocity standard deviations (STD) and mean velocities of the beams at the merging point. Another model proposed by Scharfenberg et al.[33] for crossed beam experiments at variable angles and velocities similarly defines the collision energy and resolution according to these parameters at the crossing point. Such models adequately describe collision experiments where the supersonic source pulse duration is comparable to the propagation time. However, if we assume that the phase-space distribution does not change during free flight and the beam temperatures remain equal to the initial values, which in our case were 440 and 160 mK for the two beams, the lowest overall collision temperature measured should not have reached below 350 mK (30 μeV). Moreover, the energy resolution calculated by these models would not have enabled us to resolve the shape resonances observed in Henson et al.[31]

We suggest here that the short pulsed beam dynamics, which have been overlooked in the past, enable the observation of much lower collisional energies and better resolutions than anticipated. We present a model in which the velocity STD and mean velocity of the beams at the merging (crossing) point are

Special Issue: Ron Naaman Festschrift

Received: May 8, 2013
Revised: July 25, 2013
Published: July 29, 2013

dx.doi.org/10.1021/jp4045868 | J. Phys. Chem. C 2013, 117, 22454−22461

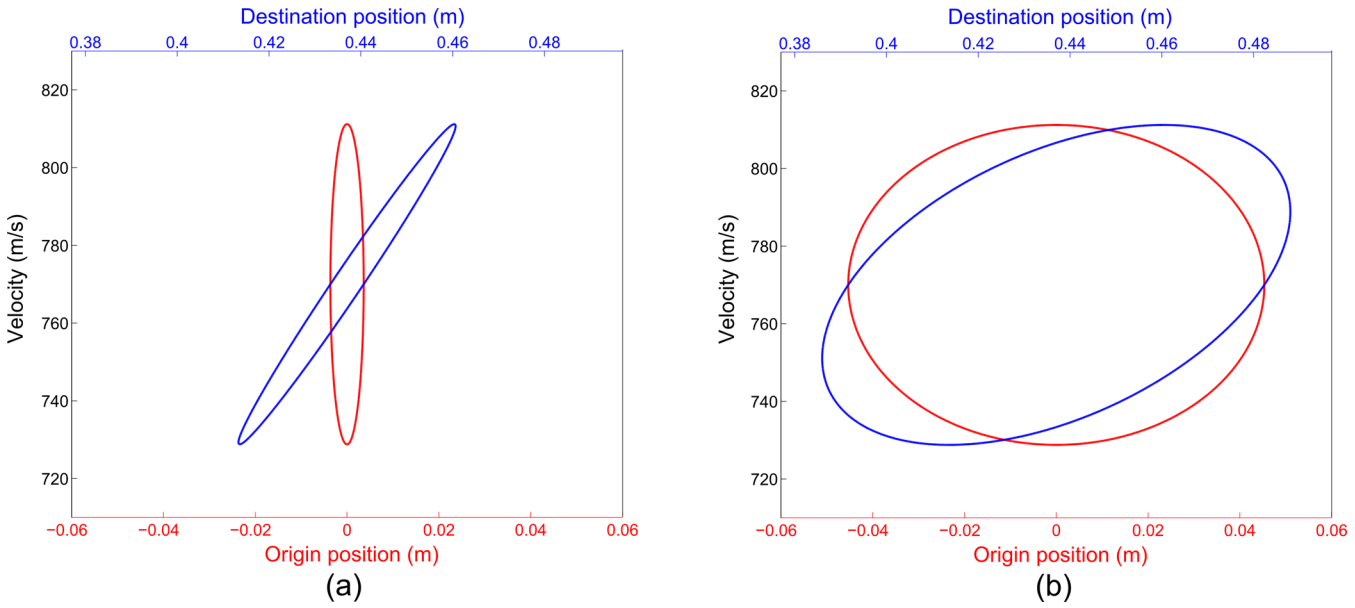

Figure 1. Shows the phase-space distributions in the longitudinal direction (eq 2.2) of a supersonic beam with a mean velocity of 770 m/s at the origin (red) and after propagating 0.44 m to the detector location (blue). The plotted circles indicate the half-maximum of the distributions in phase-space. The opening duration STDs of the beams are 4 μs (a) and 50 μs (b), where the former satisfies the condition in eq 2.5, while the latter does not. The decrease in the local velocity STD of the beam is more pronounced in (a), where the opening duration is short, in comparison to (b), where the opening duration is long.

affected by the free flight of the beams. The free propagation of a pulsed supersonic beam forms a correlation between the mean velocity and position within the cloud. In other words, faster particles are mostly situated in the front of the beam, while the slower particles tend to reside in the back of the beam. In order for the phase-space density to be conserved, the STD of the velocity distribution must decrease at any given spatial slice of the beam. The calculated resolutions of the collision energy are in line with those needed to resolve the observed features.[31] The model also indicates that shortening the detection time duration will improve the observed resolution.

Dispersion in the beam velocity distribution has been employed in the past to perform velocity dependent studies. Usually this was done by using a chopper wheel to select a short portion of transient molecules formed by a pulsed nozzle[34] or a laser ablated source.[35] In our case the pulsed opening durations of our supersonic source, the Even-Lavie valve,[36] are short enough for the dispersion to form without the need for velocity selection, as we will show.

Briefly reviewing the experimental setup from Henson et al.,[31] beams of H_2 and He were produced by Even-Lavie valves[36] at a relative angle of 10°. Immediately after the He beam valve is a dielectric barrier discharge (DBD),[37] which was used to excite the ground-state He to the metastable 2^3S level, which will be denoted by He*. The He* beam then entered a curved magnetic quadrupole guide that merged the He* with the straight H_2 beam. The H_2^+ Penning ionization reaction products were detected with a quadrupole mass spectrometer (QMS) positioned at the quadrupole guide exit. The collision energy was tuned by changing the temperature of the H_2 valve and by seeding the H_2 in noble gases from 60 meV (700 K) down to 0.9 μeV (10 mK).

2. THREE DIMENSIONAL MODEL OF BEAM DISTRIBUTION

We approach this problem from a one-dimensional perspective analyzing the distribution in the longitudinal direction first and the transverse directions later. We assume the particle distributions are normal in velocity and temporal space. The initial distribution of the beam can be described by eq 2.1, in which t and v are the time and velocity variables of the distribution, μ is the mean velocity of the beam, while σ_{v_0} and σ_t are the velocity and temporal STDs, respectively, where σ_t corresponds to the valve opening duration. To propagate the beam over a time-of-flight τ, we apply the transformation $z = \mu t + v\tau \rightarrow t = (z - v\tau)/\mu$, where z is the variable describing the position within the beam. The resulting phase-space distribution (PSD) is described by eq 2.2.

$$\rho(t, v) = \frac{1}{2\pi\sigma_{v_0}\sigma_t} \exp\left\{-\frac{(v-\mu)^2}{2\sigma_{v_0}^2} - \frac{t^2}{2\sigma_t^2}\right\} \tag{2.1}$$

$$\rho(t, v) = \rho_\tau(z, v) = \frac{1}{2\pi\sigma_{v_0}\sigma_t} \exp\left\{-\frac{(v-\mu)^2}{2\sigma_{v_0}^2} - \frac{(z-v\tau)^2}{2\mu^2\sigma_t^2}\right\} \tag{2.2}$$

In our merged beam experimental setup,[31] we generate supersonic beams using Even-Lavie valves,[36] which have opening duration STDs as short as 4 μs and the distance to the detection volume is 0.44 m. Figure 1a shows the initial PSD of the beam at the valve and the PSD at the detector for our setup's parameters plotted according to eq 2.2 for $\tau = 0$ and (0.44 m)/μ, respectively. After the propagation, the PSD has become skewed and the local velocity STD has decreased. The values for the STD and mean of the velocity distribution at a given position z are denoted by σ_v and μ_z, respectively, and are calculated explicitly in eqs 2.3 and 2.4. These values are also

dx.doi.org/10.1021/jp4045868 | J. Phys. Chem. C 2013, 117, 22454−22461

provided according to z_m, which denotes the position of the center of the beam, where $z_m = \mu\tau$.

$$\sigma_v^2 = \frac{(\mu\sigma_t\sigma_{v_0})^2}{\sigma_{v_0}^2\tau^2 + \mu^2\sigma_t^2} = \frac{(\mu^2\sigma_t\sigma_{v_0})^2}{\sigma_{v_0}^2 z_m^2 + \mu^4\sigma_t^2} \tag{2.3}$$

$$\mu_z = \frac{z\tau\sigma_{v_0}^2 + \mu^3\sigma_t^2}{\sigma_{v_0}^2\tau^2 + \mu^2\sigma_t^2} = \frac{z\mu z_m\sigma_{v_0}^2 + \mu^5\sigma_t^2}{\sigma_{v_0}^2 z_m^2 + \mu^4\sigma_t^2} \tag{2.4}$$

The local velocity STD, σ_v, becomes much smaller during free propagation if the time-of-flight satisfies eq 2.5. This condition sets the required opening duration necessary to achieve the local reduction in collision temperature. For example, if we desire a reduction of an order of magnitude in the local velocity STD at a collision distance located 0.5 m away for a beam traveling at 800 m/s with an initial velocity STD of 35 m/s, the opening duration STD must be shorter than 3 μs. When the condition in eq 2.5 is not satisfied, the correlation does not have enough time to form and there is no significant decrease in the local velocity STD, as seen in Figure 1b, in which σ_t has been taken as 50 μs, corresponding to an opening duration that can be achieved with a standard pulsed supersonic nozzle. In this case, the time evolution of the beam PSD resembles that of a continuous supersonic beam.

$$\frac{\mu\sigma_t}{\sigma_{v_0}\tau} \ll 1 \tag{2.5}$$

We now turn to calculating the distribution of the beam in the transverse directions. This is similar to the longitudinal direction, except for the calculation of the initial beam size, which cannot be estimated by the valve opening duration, because the mean velocity in this direction must be zero. Instead the valve orifice size is used to approximate the STD of the initial spatial distribution denoted by σ_x. The resulting PSD in the $x(y)$ direction is given by eq 2.6, where v_x and x_0 are the variables for the velocity and initial position respectively, while σ_{v_0} is the initial velocity STD. Applying the transformation $x = x_0 + v_x\tau$, where x is the variable for the position after propagation in time, τ, we find that the PSD is given by eq 2.7. The local STD and mean of the velocity distribution in the $x(y)$ direction are given by eqs 2.8 and 2.9, respectively.

$$\rho(x_0, v_x) = \frac{1}{2\pi\sigma_{v_0}\sigma_x}\exp\left\{-\frac{v_x^2}{2\sigma_{v_0}^2} - \frac{x_0^2}{2\sigma_x^2}\right\} \tag{2.6}$$

$$\rho(x_0, v_x) = \rho_\tau(x, v_x) = \frac{1}{2\pi\sigma_{v_0}\sigma_x}\exp\left\{-\frac{v_x^2}{2\sigma_{v_0}^2} - \frac{(x - v_x\tau)^2}{2\sigma_x^2}\right\} \tag{2.7}$$

$$\sigma_{v_x}^2 = \frac{(\sigma_x\sigma_{v_0})^2}{\sigma_{v_0}^2\tau^2 + \sigma_x^2} = \frac{(\mu\sigma_x\sigma_{v_0})^2}{\sigma_{v_0}^2 z_m^2 + \mu^2\sigma_x^2} \tag{2.8}$$

$$\mu_x = \frac{x\tau\sigma_{v_0}^2}{\sigma_{v_0}^2\tau^2 + \sigma_x^2} = \frac{x\mu z_m\sigma_{v_0}^2}{\sigma_{v_0}^2 z_m^2 + \mu^2\sigma_x^2} \tag{2.9}$$

The He* beam that enters the quadrupole guide does not freely propagate during the entire time-of-flight. Because the guide potential is constant in the longitudinal direction and there is a constant magnetic field gradient trap in the transverse direction, we estimate that the longitudinal direction is unaffected, while in the transverse direction the expansion is halted and the distribution remains static. Thus, in order to compensate for the quadrupole guide, we shorten the time-of-flight for the transverse direction by the time traveled in the guide for the corresponding beam. The DBD creates a short He* burst at the valve reducing the opening duration STD to about 1 μs.

3. LOCAL RESOLUTION IN MERGED BEAM COLLISIONS

To calculate the collision energy distribution, we must first find the distribution of $(\Delta v)^2 = |\vec{v}_1 - \vec{v}_2|^2 = (\Delta v_x)^2 + (\Delta v_y)^2 + (\Delta v_z)^2$, where $\Delta v_i = v_{1,i} - v_{2,i}$. The velocity indices 1 and 2 denote the beam to which the velocity corresponds, and the index $i \in \{x,y,z\}$ is used to denote the Cartesian directions. The variables describing the velocity differences, Δv_i, are independent and therefore we can analyze the distribution on each axis separately. We take the distribution of $v_{n,i}$ $n \in \{1,2\}$ according to the normal distributions developed in section 2. Because Δv_i is composed of two independent normally distributed variables, its distribution must also be normal and is given by eq 3.1 for a specified position r_i. The definition used for a normal distribution is $N_x(\mu,\sigma) = (2\pi\sigma^2)^{-1/2}\exp\{-(x-\mu)^2/(2\sigma^2)\}$, where μ is the mean and σ is the STD.

$$P_{r_i}(\Delta v_i) = N_{\Delta v_i}(\mu_{1,i}(r_i) - \mu_{2,i}(r_i), \sqrt{\sigma_{v_{1,i}}^2 + \sigma_{v_{2,i}}^2}) \tag{3.1}$$

The local STD of the relative velocities, Δv_i, is determined according to eqs 2.3 and 2.8, and the mean is determined according to eqs 2.4 and 2.9 for the longitudinal and transverse directions, respectively. The expectation value and STD of the collision energy distribution are calculated according to eqs 3.2, 3.3, and 3.4, for normally distributed random variables. The resulting energy STD is given by eq 3.5 and the expectation value of the energy distribution is given by eq 3.6. The reduced mass of the colliding pair is denoted by m.

$$\mathrm{Var}[(\Delta v_i)^2] = \langle(\Delta v_i)^4\rangle - \langle(\Delta v_i)^2\rangle^2 = 4\langle\Delta v_i\rangle^2\sigma_{\Delta v_i}^2 + 2\sigma_{\Delta v_i}^4 \tag{3.2}$$

$$\mathrm{Var}[(\Delta v)^2] = \sum_i \mathrm{Var}[(\Delta v_i)^2] \tag{3.3}$$

$$\langle x^2\rangle = \frac{m}{2}\int x^2 N_x(\mu,\sigma)\mathrm{d}x = \mu^2 + \sigma^2 \tag{3.4}$$

$$\Delta E(\vec{r}) = \frac{m}{2}\sqrt{\sum_i [4(\mu_{1,i}(r_i) - \mu_{2,i}(r_i))^2(\sigma_{v_{1,i}}^2 + \sigma_{v_{2,i}}^2) + 2(\sigma_{v_{1,i}}^2 + \sigma_{v_{2,i}}^2)^2]} \tag{3.5}$$

$$\langle E\rangle(\vec{r}) = \frac{m}{2}\sqrt{\sum_i [(\mu_{1,i}(r_i) - \mu_{2,i}(r_i))^2 + \sigma_{v_{1,i}}^2 + \sigma_{v_{2,i}}^2]} \tag{3.6}$$

The energy resolution, which is defined as $\Delta E/\langle E\rangle$, where $\langle E\rangle$ is the expectation value of the energy, can be calculated analytically for any location in the merged beams. The solid black curve in Figure 4 shows the energy resolution as a function of the expectation value at the center of the overlapped beams.

dx.doi.org/10.1021/jp4045868 | J. Phys. Chem. C 2013, 117, 22454−22461

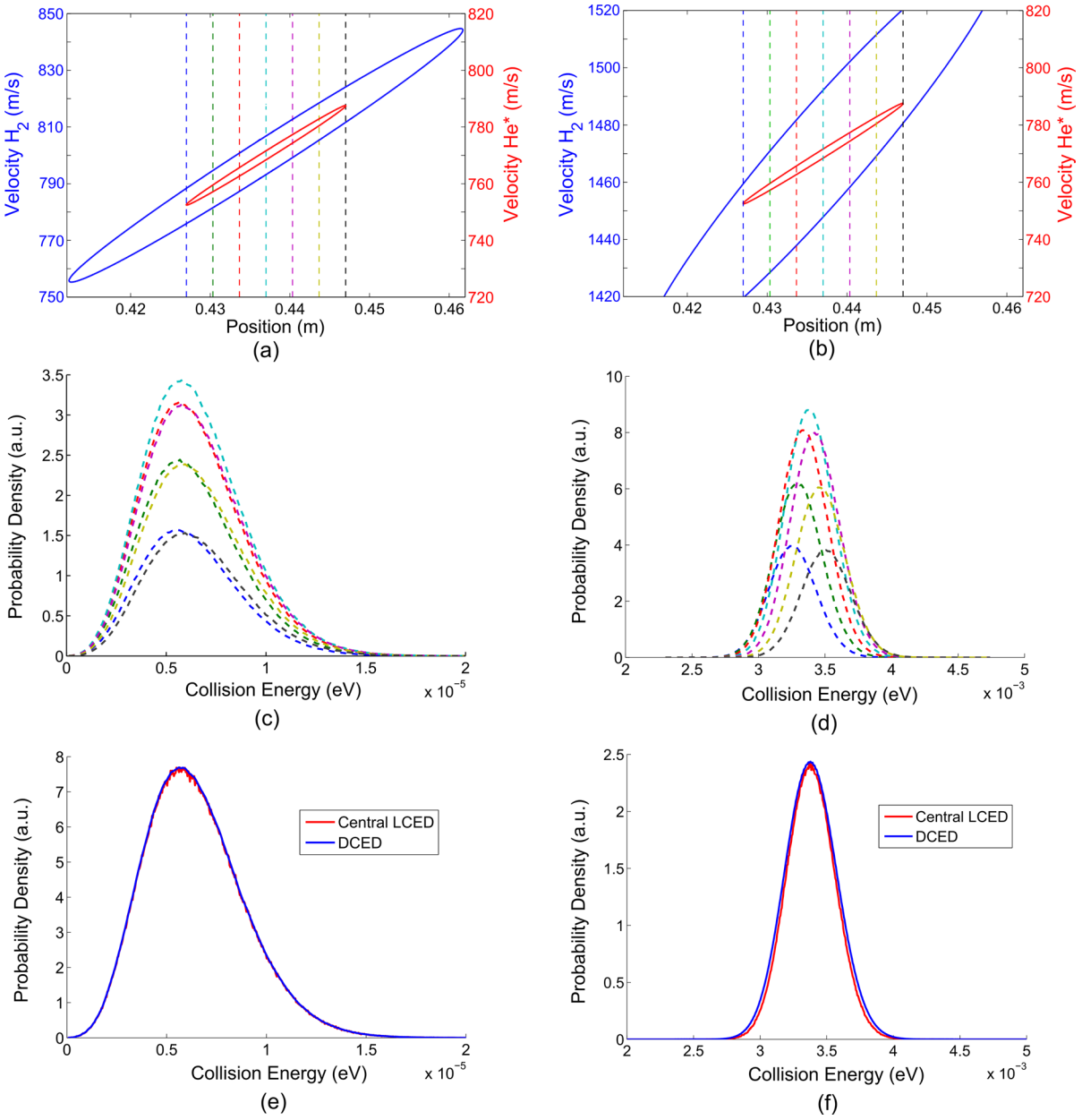

Figure 2. (a, c, and e) Low relative mean velocity case, where v_{H_2} = 800 m/s and σ_{v_0} = 38 m/s; (b, d, and f) high relative mean velocity case, where v_{H_2} = 1470 m/s and σ_{v_0} = 62 m/s. (a, b) Phase-space distribution on the longitudinal axis at half-maximum of the He* beam (red), which has a mean velocity of 770 m/s and initial velocity STD σ_{v_0} = 15 m/s, merged with the H_2 beam after the beams have freely propagated to 0.44 m. The local collision energy distributions or LCEDs (c, d) within a 2 cm long detection volume are weighted according to the beam densities at their respective locations, and their respective positions in the detection volume are indicated by the color-coded vertical dashed lines in (a) and (b). The overall detected collision energy distribution or DCED (e, f, blue) is formed from the combination of the LCEDs. The DCED is very similar to the central location LCED (red) in the low relative mean velocity case, while it is noticeably wider in the high relative mean velocity case. The valve opening duration STDs used in the calculations was 1 μs for the He* beam and 4 μs for the H_2 beam.

4. DETECTED RESOLUTION OF MERGED BEAMS

In the previous section we derived an expression for the mean and STD of the collision energy as a function of the time-of-flight and position. However, the experimentally achievable resolution and mean collision energy depend on the particular implementation of the detection system. Broadly we can divide them into two categories. The first category, which includes time-sliced detection while integrating over a finite detection volume, is discussed in section 4.1, and the second, which includes detection in a finite volume while integrating the signal over the time when the beams merge, is discussed in section 4.2. In our experiment[31] products were detected using a quadrupole mass spectrometer (QMS), with a well-defined ion collection volume and with the ion current integrated over time. As such, this detection scheme corresponds to the category of time-integrated detection in a finite region.

4.1. Time-Sliced Detection in a Finite Region. In a time-sliced detection scheme, the colliding particles that contribute to the measured signal originate at a specific time interval, but from any point within the detection volume. The time-slice

dx.doi.org/10.1021/jp4045868 | J. Phys. Chem. C 2013, 117, 22454−22461

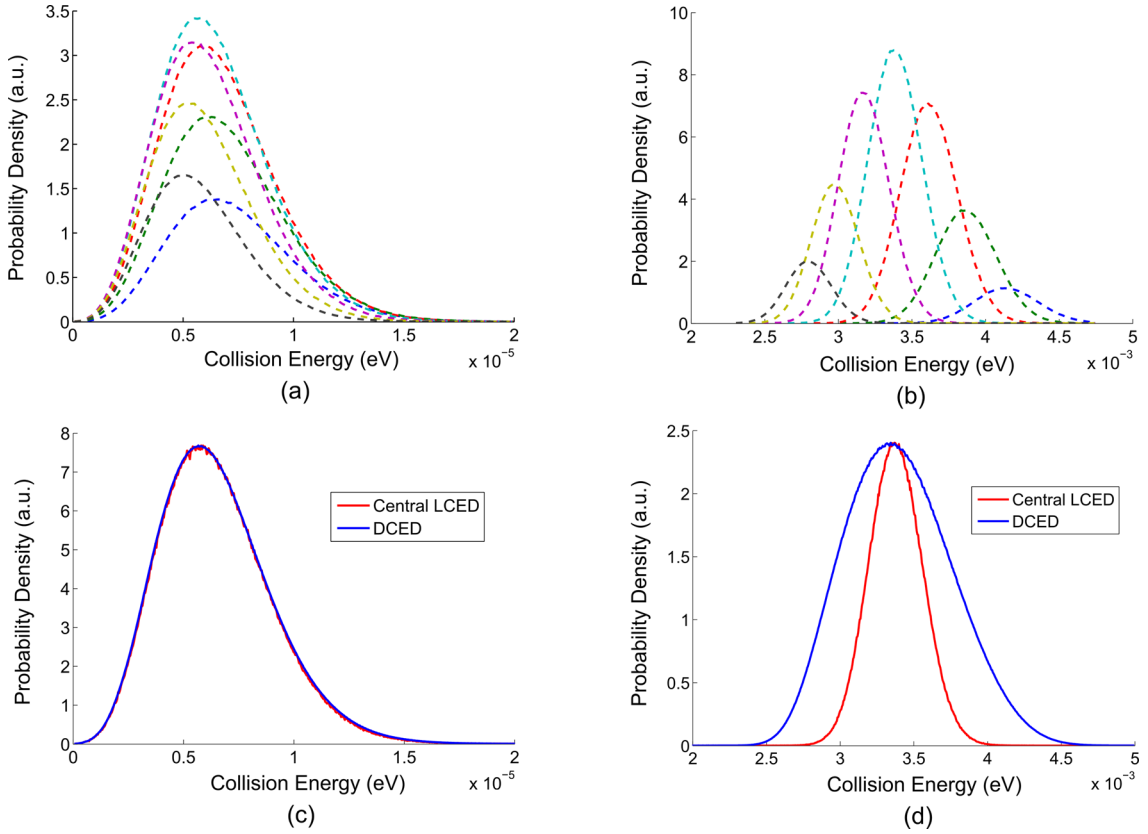

Figure 3. (a, c) Low relative mean velocity case, where v_{H_2} = 800 m/s and σ_{v_0} = 38 m/s; (b, d) high relative mean velocity case, where v_{H_2} = 1470 m/s and σ_{v_0} = 32 m/s. The local collision energy distributions or LCEDs (a, b) at different times and locations along the propagation axis within the 2 cm long detection volume, are normalized according to their respective beam densities. The overall detected collision energy distribution or DCED (c, d, blue) is formed from the combination of the LCEDs. The DCED is very similar to the central location and time LCED (red) in the low relative mean velocity case, while it is almost twice as wide in the high relative mean velocity case. The seven LCED time-slices in (a) and (b) were chosen linearly in ascending order in the 52 μs window when the center of the He* beam, which travels at 770 m/s with an initial velocity STD σ_{v_0} = 15 m/s, is located inside the detection volume and their respective locations are indicated by the color-coded dashed vertical lines in Figure 2a and b, respectively. The valve opening duration STDs used in the calculations was 1 μs for the He* beam and 4 μs for the H_2 beam.

chosen in order to maximize the signal is when both beams merge in the middle of the detection volume.

The collision energy distribution is simulated numerically for each relative mean velocity between the beams. This is done by generating sets of the values $\{\Delta v_x, \Delta v_y, \Delta v_z\}$ according to the respective distributions of Δv_i given by eq 3.1. The STDs $\sigma_{vn,i}$ and means $\mu_{n,i}(r_i)$ of these distributions at each location within the detection volume are given by eqs 2.3 and 2.4 for the longitudinal direction and eqs 2.8 and 2.9 for the transverse directions. The corresponding collision energy for each set is $E = m/2((\Delta v_x)^2 + (\Delta v_y)^2 + (\Delta v_z)^2)$. The generated energies are distributed according to the collision energy distribution at the given location, which we call the "local collision energy distribution" (LCED).

The next step is to find the LCEDs at different locations within the detection volume and then combine them to form a set of energies distributed according to the overall "detected collision energy distribution" (DCED). The impact of each LCED on the overall energy distribution is weighted according to the relative density of the beams at the location of the LCED. The local density of each beam is determined by the product of the densities on each axis. The density on each axis is given by the PSDs in eqs 2.2 and 2.7 for the longitudinal and transverse directions, respectively, after integrating out the velocity. The product of the local densities of the beams determines the weight of each LCED.

To explain the significance of the finite collection region, we will discuss two separate examples; the two beams merge at a low relative mean velocity of 30 m/s and at a high relative mean velocity of 700 m/s. In our measurements in Henson et al.,[31] the velocity STD of the H_2 beam was 38 m/s for the low relative velocity case and 62 m/s for the high relative velocity case. In Figure 2a the PSDs on the longitudinal axis of the two merged beams are plotted for the low relative velocity case. The two PSDs are skewed at approximately the same angle. In Figure 2c several weighted LCEDs are plotted, whose corresponding locations on the z axis are indicated by the color coded dashed lines in Figure 2a. As one can see, the DCED (Figure 2e) is very similar to the central location LCED and is not widened by the off-center LCEDs. This is a direct result of PSDs being relatively parallel (Figure 2a), such that the mean collision energies of the off-center LCEDs do not vary enough compared to the local STD, to widen the DCED. This is no longer true for the high relative mean velocity case where the angle between the PSDs (Figure 2b) is clearly visible. In Figure 2d, the LCEDs are plotted in the same scheme as in Figure 2c, but in this case, the DCED is noticeably wider than the central LCED at the half-maximum (Figure 2f). The STD

dx.doi.org/10.1021/jp4045868 | J. Phys. Chem. C 2013, 117, 22454−22461

of the DCED is likewise larger than the STDs of the LCEDs, as will be discussed in section 5.

The QMS ion detection volume was cylindrical in shape with a length of 2 cm and a radius of 5 mm, which are the values used in the calculations. The locations taken in the calculation of the DCED were on the z axis disregarding the changes in mean energy in the transverse direction. This approximation is valid since at the maximal transverse radius of 5 mm the condition $(\mu_{1,i}(r_i = 5\text{ mm}) - \mu_{2,i}(r_i = 5\text{ mm}))^2/(\sigma^2_{v_{1,i}} + \sigma^2_{v_{2,i}}) \ll 1; i \in \{x,y\}$ is satisfied, which means that the mean collision energy given by eq 3.6 varies negligibly compared to the STD given by eq 3.5. In fact, for the worst case parameters where the beam velocities are equal we find that $(\langle E\rangle(r_x = 5\text{ mm}) - \langle E\rangle(r_x = 0))/\Delta E(r_x = 0) < 10^{-4}$.

By decreasing the size of the detection volume, the detected energy resolution would improve at the price of the number of products collected, though for this case the improvement is not substantial. In other words, the 2 cm length of our detection volume is very close to optimal for a merged beam setup at the beam velocities used. We will show, however, that this is no longer true for a time-integrated detection implementation in section 4.2.

4.2. Time-Integrated Detection in Finite Region. In a time-integrated detection scheme, the signal can originate at any time as well as from any point in the detection volume. The DCED is therefore determined in the same way as in section 4.1, except that the weighted LCEDs are taken from different time-slices as well as different locations. Figure 3a and b show several such LCEDs on the longitudinal axis of the merged beams in the low and high relative mean velocity cases, respectively. The DCED for the low relative velocity case is also similar to the central location and time LCED (Figure 3c), which originates from the time-slice when the centers of the two beams meet in the middle of the detector.

In the high relative velocity case we see the same broadening effect of the DCED as in the time-sliced implementation, except that it is more pronounced (Figure 3d). The mean energy of the off-center LCEDs varies much more in this case than in the equivalent time-sliced case. This effect can be seen intuitively by "moving" the H_2 phase-space distribution in Figure 2b on the position axis over the He* beam distribution and looking at the mean velocity at the densest overlap locations. The DCED is more than twice as wide as the central LCED at the half-maximum. This means that by decreasing the detection duration, the detected energy resolution would improve at the price of the number of products observed.

5. DETECTION METHOD COMPARISON

We have shown in section 4 that the two different detection implementations discussed have an impact on the resolution observed. The optimal resolution in this kind of merged beam setup will always be achieved with a small temporal and spatial detection system, since it corresponds directly to the local collision energy STD. At low relative mean velocities the resolution is not greatly affected while at high relative mean velocities the difference is substantial. Figure 4 shows a comparison of the resolutions expected for each implementation. The velocity STD of the H_2 beam was taken as $\sigma_{v_0} = 0.034 \cdot v_{H_2} + 12.35$ m/s, from a fit of the velocity STDs measured in Henson et al.[31]

The dashed purple curve in Figure 4 shows the resolution without the phase-space correlation effect, which lowers the

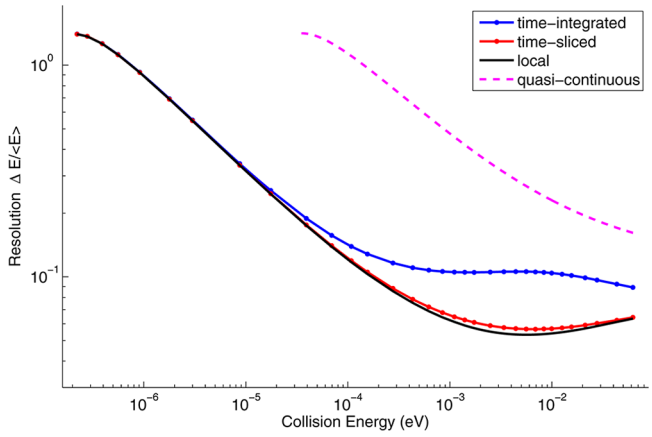

Figure 4. Comparison of resolutions calculated according to the different detection implementations discussed in section 4, and the quasi-continuous nozzle resolution as a function of the collision energy. The local resolution (black-solid) is determined analytically according to eqs 3.5 and 3.6, and corresponds to a detector with an infinitesimal temporal and spatial detection volume. The time-sliced resolution (red) is determined numerically according to section 4.1, and corresponds to a detector with a short detection time-slice and 2 cm long detection volume. The time-integrated resolution (blue) is determined numerically according to section 4.2 and corresponds to a detector that perpetually collects products in a 2 cm long detection volume. The quasi-continuous or continuous nozzle resolution (dashed-purple) is determined by the initial velocity STDs, disregarding the correlation formed in the phase-space distribution during free propagation. The markers on the time-sliced and time-integrated resolution lines indicate the numerically calculated values.

local velocity STD, as described in section 2 and as would be achieved with quasi-continuous or continuous nozzles. The resolution in this case is up to an order of magnitude worse. The Penning ionization reaction rate results in Henson et al.,[31] which are shown in Figure 5, and specifically the energy differences between the resonances detected indicate that these resonances would not have been resolvable without the phase-space correlation effect. The resonance at 0.2 meV has a resolution of 0.88 for a quasi-continuous nozzle. Clearly, the

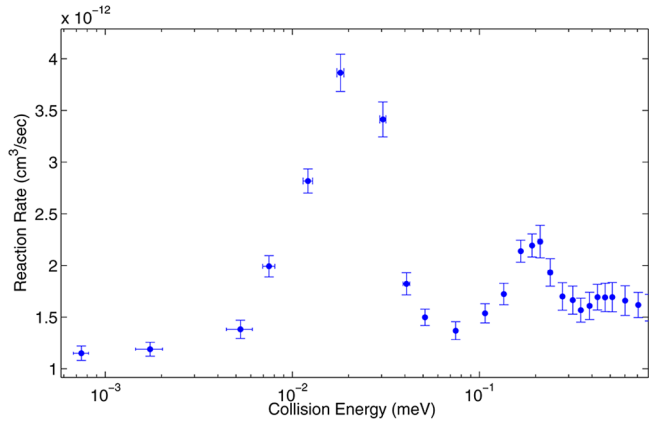

Figure 5. Penning ionization reaction rate results for He* + $H_2 \rightarrow$ He + $H_2^+ + e^-$ in the energy range which includes the shape resonances as published in Henson et al.[31] The two resonances are located at the energies 0.02 and 0.2 meV. For a mean collision energy of 0.2 meV, the predicted collision energy STD attained with a quasi-continuous nozzle is 0.17 meV, as shown in Figure 4. Resolving the resonance located at 0.02 meV would have been difficult with such a nozzle.

dx.doi.org/10.1021/jp4045868 | J. Phys. Chem. C 2013, 117, 22454−22461

width of the observed peak is narrower than the predicted STD of 0.17 meV by an order of magnitude. Moreover, the resonance at 0.02 meV is located about one standard deviation away, which would have made it very difficult to resolve.

As expected, the resolution improves by up to a factor of 2 at high collision energies between time-integrated and time-sliced detection implementations. The difference between the time-sliced and local resolution is not substantial at any collision energy, indicating that the 2 cm length of the detection volume is close to optimal with respect to the size of the system and velocities of the beams.

At collision energies above 7 meV, the gap between the time-integrated and time-sliced detection cases gets smaller. The velocity of the H_2 beam becomes so fast, above 2700 m/s, that the correlation in phase-space does not have enough time to form. This can be described formally by the condition (eq 2.5) for the decrease of velocity STD, which begins to break down. The high energy region is also where reaction rates are relatively high in Henson et al.,[31] such that it may be possible to concede some of the signal intensity for improved resolution.

The lowest attainable collision energy in the merged beam system is constrained by how well the two beams are merged. For example, if the angle between the beams is 1° after the merging process and the relative velocity between the beams is zero, then the collision energy will be about 1.5 μeV, which is more than six times the "perfectly" merged minimal collision energy. However, because both beams propagate along the same axis, a merging angle of less than 0.7° can easily be achieved using an aperture. The corresponding lowest collision energy is less than 0.86 μeV (10 mK), and the resolution is uncompromised.

6. CONCLUSIONS

We have shown that during free flight propagation of a pulsed supersonic beam, the local velocity STD decreases, due to correlations formed in the PSD. This decrease becomes significant when the opening time of the valve is short compared to the overall propagation time (eq 2.5). The proposed model predicts that in the example merged beam system the observed collision energies will be 2 orders of magnitude lower and the resolution will be an order of magnitude better than in the case where the beam distribution is constant, which corresponds to a quasi-continuous beam. These predictions fit well with the observed Penning ionization reaction rates in Henson et al.,[31] with respect to the shape of the resonant peaks and their energy positions. Another prediction shows that by adapting the detection system, such that it detects products during short time-slices, the resolution will improve by up to a factor of two.

The short opening duration valves provide an added advantage to a merged beam system enabling the measurement of collisions well into the cold regime, down to 10 mK. Understanding this model may allow even colder temperatures to be reached in a merged beam setup, by increasing the time-of-flight of the beams, for example, or lead to completely different systems that leverage the PSD correlation formed to their advantage.

AUTHOR INFORMATION

Corresponding Author

*E-mail: edn@weizmann.ac.il.

Notes

The authors declare no competing financial interest.

ACKNOWLEDGMENTS

This research was made possible, in part, by the historic generosity of the Harold Perlman Family. E.N. acknowledges support from the Israel Science Foundation.

REFERENCES

(1) Krems, R. V. Cold Controlled Chemistry. *Phys. Chem. Chem. Phys.* **2008**, *10*, 4079−92.
(2) Wigner, E. On the Behavior of Cross Sections Near Thresholds. *Phys. Rev.* **1948**, *73*, 1002−1009.
(3) Herschbach, D. R. In *Reactive Scattering in Molecular Beams*; Ross, J., Ed.; John Wiley & Sons, Inc.: Hoboken, NJ, 1966; Vol. *10*.
(4) Lee, Y. T.; McDonald, J. D.; LeBreton, P. R.; Herschbach, D. R. Molecular-Beam Kinetics: Evidence for Short-Range Attraction in Halogen Atom−Molecule Exchange Reactions. *J. Chem. Phys.* **1968**, *49*, 2447.
(5) Lee, Y. T.; McDonald, J. D.; LeBreton, P. R.; Herschbach, D. R. Molecular Beam Reactive Scattering Apparatus with Electron Bombardment Detector. *Rev. Sci. Instrum.* **1969**, *40*, 1402.
(6) Schutte, A.; Bassi, D.; Tommasini, F.; Scoles, G. Orbiting Resonances in the Scattering of H Atoms by Mercury at Thermal Energies. *Phys. Rev. Lett.* **1972**, *29*, 979−982.
(7) Toennies, J. P.; Welz, W.; Wolf, G. Observation of Orbiting Resonances in the Integral Cross Section of H-Xe. *J. Chem. Phys.* **1974**, *61*, 2461.
(8) Toennies, J. P.; Welz, W.; Wolf, G. Molecular Beam Scattering Studies of Orbiting Resonances and the Determination of van der Waals Potentials for H−Ne, Ar, Kr, and Xe and for H2−Ar, Kr, and Xe. *J. Chem. Phys.* **1979**, *71*, 614.
(9) Rowe, B. R.; Dupeyrat, G.; Marquette, J. B.; Gaucherel, P. Study of the Reactions $N^+_2 + 2N_2 \rightarrow N^+_4 + N_2$ and $O^+_2 + 2O_2 \rightarrow O^+_4 + O_2$ from 20 to 160 K by the CRESU Technique. *J. Chem. Phys.* **1984**, *80*, 4915.
(10) Smith, I. W. M. Reactions at Very Low Temperatures: Gas Kinetics at a New Frontier. *Angew. Chem., Int. Ed.* **2006**, *45*, 2842−61.
(11) Berteloite, C.; Lara, M.; Bergeat, A.; Le Picard, S. D.; Dayou, F.; Hickson, K. M.; Canosa, A.; Naulin, C.; Launay, J.-M.; Sims, I. R.; Costes, M. Kinetics and Dynamics of the $S(^1D_2) + H_2 \rightarrow SH + H$ Reaction at Very Low Temperatures and Collision Energies. *Phys. Rev. Lett.* **2010**, *105*, 203201.
(12) Doyle, J.; Friedrich, B.; Kim, J.; Patterson, D. Buffer-Gas Loading of Atoms and Molecules into a Magnetic Trap. *Phys. Rev. A* **1995**, *52*, R2515−R2518.
(13) Singh, V.; Hardman, K.; Tariq, N.; Lu, M.-J.; Ellis, A.; Morrison, M.; Weinstein, J. Chemical Reactions of Atomic Lithium and Molecular Calcium Monohydride at 1 K. *Phys. Rev. Lett.* **2012**, *108*, 203201.
(14) Bethlem, H.; Berden, G.; Meijer, G. Decelerating Neutral Dipolar Molecules. *Phys. Rev. Lett.* **1999**, *83*, 1558−1561.
(15) Van de Meerakker, S. Y. T.; Meijer, G. Collision Experiments with Stark-Decelerated Beams. *Faraday Discuss.* **2009**, *142*, 113.
(16) Gilijamse, J. J.; Hoekstra, S.; van de Meerakker, S. Y. T.; Groenenboom, G. C.; Meijer, G. Near-Threshold Inelastic Collisions Using Molecular Beams with a Tunable Velocity. *Science* **2006**, *313*, 1617−20.
(17) Kirste, M.; Wang, X.; Schewe, H. C.; Meijer, G.; Liu, K.; van der Avoird, A.; Janssen, L. M. C.; Gubbels, K. B.; Groenenboom, G. C.; van de Meerakker, S. Y. T. Quantum-State Resolved Bimolecular Collisions of Velocity-Controlled OH with NO Radicals. *Science* **2012**, *338*, 1060−3.
(18) Sawyer, B. C.; Stuhl, B. K.; Yeo, M.; Tscherbul, T. V; Hummon, M. T.; Xia, Y.; Klos, J.; Patterson, D.; Doyle, J. M.; Ye, J. Cold Heteromolecular Dipolar Collisions. *Phys. Chem. Chem. Phys.* **2011**, *13*, 19059−66.

(19) Narevicius, E.; Libson, A.; Parthey, C. G.; Chavez, I.; Narevicius, J.; Even, U.; Raizen, M. G. Stopping Supersonic Beams with a Series of Pulsed Electromagnetic Coils: An Atomic Coilgun. *Phys. Rev. Lett.* **2008**, *100*, 093003.
(20) Vanhaecke, N.; Meier, U.; Andrist, M.; Meier, B. H.; Merkt, F. Multistage Zeeman Deceleration of Hydrogen Atoms. *Phys. Rev. A* **2007**, *75*, 031402.
(21) Fulton, R.; Bishop, A.; Barker, P. Optical Stark Decelerator for Molecules. *Phys. Rev. Lett.* **2004**, *93*, 243004.
(22) Gupta, M.; Herschbach, D. Slowing and Speeding Molecular Beams by Means of a Rapidly Rotating Source. *J. Phys. Chem. A* **2001**, *105*, 1626−1637.
(23) Lavert-Ofir, E.; Gersten, S.; Henson, A. B.; Shani, I.; David, L.; Narevicius, J.; Narevicius, E. A Moving Magnetic Trap Decelerator: A New Source of Cold Atoms and Molecules. *New J. Phys.* **2011**, *13*, 103030.
(24) Wiederkehr, A. W.; Motsch, M.; Hogan, S. D.; Andrist, M.; Schmutz, H.; Lambillotte, B.; Agner, J. A.; Merkt, F. Multistage Zeeman Deceleration of Metastable Neon. *J. Chem. Phys.* **2011**, *135*, 214202.
(25) Shagam, Y.; Narevicius, E. Density and Phase-Space Compression of Molecular Gases in Magneto-Electrostatic Traps. *Phys. Rev. A* **2012**, *85*, 053406.
(26) Narevicius, E.; Bannerman, S. T.; Raizen, M. G. Single-Photon Molecular Cooling. *New J. Phys.* **2009**, *11*, 055046.
(27) Willitsch, S.; Bell, M.; Gingell, A.; Procter, S.; Softley, T. Cold Reactive Collisions between Laser-Cooled Ions and Velocity-Selected Neutral Molecules. *Phys. Rev. Lett.* **2008**, *100*, 043203.
(28) Ospelkaus, S.; Ni, K.-K.; Wang, D.; de Miranda, M. H. G.; Neyenhuis, B.; Quéméner, G.; Julienne, P. S.; Bohn, J. L.; Jin, D. S.; Ye, J. Quantum-State Controlled Chemical Reactions of Ultracold Potassium-Rubidium Molecules. *Science* **2010**, *327*, 853−7.
(29) Mazely, T. L.; Smith, M. A. Gas Phase Reaction Rates of C^+ with O_2, NO, and N_2O near 0.6 K. *Chem. Phys. Lett.* **1988**, *144*, 563.
(30) Hall, F. H. J.; Willitsch, S. Millikelvin Reactive Collisions between Sympathetically Cooled Molecular Ions and Laser-Cooled Atoms in an Ion-Atom Hybrid Trap. *Phys. Rev. Lett.* **2012**, *109*, 233202.
(31) Henson, A. B.; Gersten, S.; Shagam, Y.; Narevicius, J.; Narevicius, E. Observation of Resonances in Penning Ionization Reactions at Sub-Kelvin Temperatures in Merged Beams. *Science* **2012**, *338*, 234−238.
(32) Wei, Q.; Lyuksyutov, I.; Herschbach, D. Merged-Beams for Slow Molecular Collision Experiments. *J. Chem. Phys.* **2012**, *137*, 054202.
(33) Scharfenberg, L.; van de Meerakker, S. Y. T.; Meijer, G. Crossed Beam Scattering Experiments with Optimized Energy Resolution. *Phys. Chem. Chem. Phys.* **2011**, *13*, 8448−56.
(34) Kay, B. D.; Raymond, T. D.; Rice, J. K. Time-of-Flight Characterization of Pulsed Supersonic Helium Free-Jet Expansions. *Rev. Sci. Instrum.* **1986**, *57*, 2266.
(35) Willis, P. A.; Stauffer, H. U.; Hinrichs, R. Z.; Davis, H. F. Rotatable Source Crossed Molecular Beams Apparatus with Pulsed Ultraviolet/Vacuum Ultraviolet Photoionization Detection. *Rev. Sci. Instrum.* **1999**, *70*, 2606.
(36) Even, U.; Jortner, J.; Noy, D.; Lavie, N.; Cossart-Magos, C. Cooling of Large Molecules below 1 K and He Clusters Formation. *J. Chem. Phys.* **2000**, *112*, 8068.
(37) Luria, K.; Lavie, N.; Even, U. Dielectric Barrier Discharge Source for Supersonic Beams. *Rev. Sci. Instrum.* **2009**, *80*, 104102.